scientific reports

Check for updates

OPEN

An evaluation of the self-assembly enhancing properties of cell-derived hexameric amyloid-β

Devkee M. Vadukul[1,4], Céline Vrancx[1], Pierre Burguet[2], Sabrina Contino[1], Nuria Suelves[1], Louise C. Serpell[3], Loïc Quinton[2] & Pascal Kienlen-Campard[1]✉

A key hallmark of Alzheimer's disease is the extracellular deposition of amyloid plaques composed primarily of the amyloidogenic amyloid-β (Aβ) peptide. The Aβ peptide is a product of sequential cleavage of the Amyloid Precursor Protein, the first step of which gives rise to a C-terminal Fragment (C99). Cleavage of C99 by γ-secretase activity releases Aβ of several lengths and the Aβ42 isoform in particular has been identified as being neurotoxic. The misfolding of Aβ leads to subsequent amyloid fibril formation by nucleated polymerisation. This requires an initial and critical nucleus for self-assembly. Here, we identify and characterise the composition and self-assembly properties of cell-derived hexameric Aβ42 and show its assembly enhancing properties which are dependent on the Aβ monomer availability. Identification of nucleating assemblies that contribute to self-assembly in this way may serve as therapeutic targets to prevent the formation of toxic oligomers.

Alzheimer's disease (AD) is a neurodegenerative disease characterised by the deposition of extracellular amyloid plaques in the brain which are primarily composed of the self-assembled amyloid-β (Aβ) peptide[1]. The self-assembly process of Aβ has been the focus of much research, however, it is still unclear how this relates to disease pathology. Aβ is a product of sequential cleavage of the Amyloid Precursor Protein (APP) in the amyloidogenic pathway where APP is first cleaved by β-secretase at the N-terminus of Aβ. The two products of this are soluble APP-β (sAPPβ) and a C-terminal fragment (CTF) consisting of 99 amino acids (C99). C99 is further cleaved by γ-secretase, beginning with a proteolytic cut at the ε site, to free the C-terminal APP intracellular domain (AICD), and release Aβ of varying lengths ranging from Aβ49-38[2–4].

Although extracellular Aβ plaques found in AD brains are primarily composed of highly ordered cross-β mature amyloid fibrils[5–7], soluble forms of Aβ have shown a much greater correlation with cognitive decline and neurodegeneration in AD patients[8,9]. Due to this, it is now widely accepted that pre-fibrillar spherical/globular Aβ oligomers are neurotoxic entities. In particular, several Aβ42 oligomers of different assembly sizes and conformations have been identified as being cytotoxic[7,10–18].

Oligomers are formed as intermediary assemblies during amyloid formation, the mechanism of which is via nucleated polymerisation[19]. There is first the nucleation or lag phase where the monomer precursor is either in an unfolded, partially folded or natively folded state and undergoes usually unfavourable self-association to form nuclei that are critical for further self-assembly[20]. This critical nucleus is defined as the smallest assembly size that grows faster by the addition of monomers, than dissociates back to smaller assemblies including monomers[21]. Once the critical nucleus has been formed, there is a rapid formation of fibrils by the addition of monomers. This is the elongation phase and fibril formation in this way is known as primary nucleation. The formation of these nuclei is therefore crucial in the generation of amyloid and the identification of these structures will ultimately aid our understanding of amyloid assembly and pathology.

One likely nucleus of Aβ42 assembly has been suggested to be a hexameric assembly[20,22–26]. It has been shown that the formation of hexameric Aβ42 is an early event in the self-assembly pathway[23,24,27,28] and the identification of several multimers of hexamers e.g. Aβ derived diffusible ligands (ADDLs), Aβ*56 and globulomers, provide a

[1]Alzheimer Research Group, Molecular and Cellular Division (CEMO), Institute of Neuroscience, Université Catholique de Louvain, Brussels, Belgium. [2]Mass Spectrometry Laboratory, MolSys Research Unit, University of Liège, Liège, Belgium. [3]Sussex Neuroscience, School of Life Sciences, University of Sussex, Falmer, Brighton, East Sussex BN1 9QG, UK. [4]Present address: Molecular Sciences Research Hub (MSRH), Department of Chemistry, Imperial College London, London, UK. ✉email: pascal.kienlen-campard@uclouvain.be

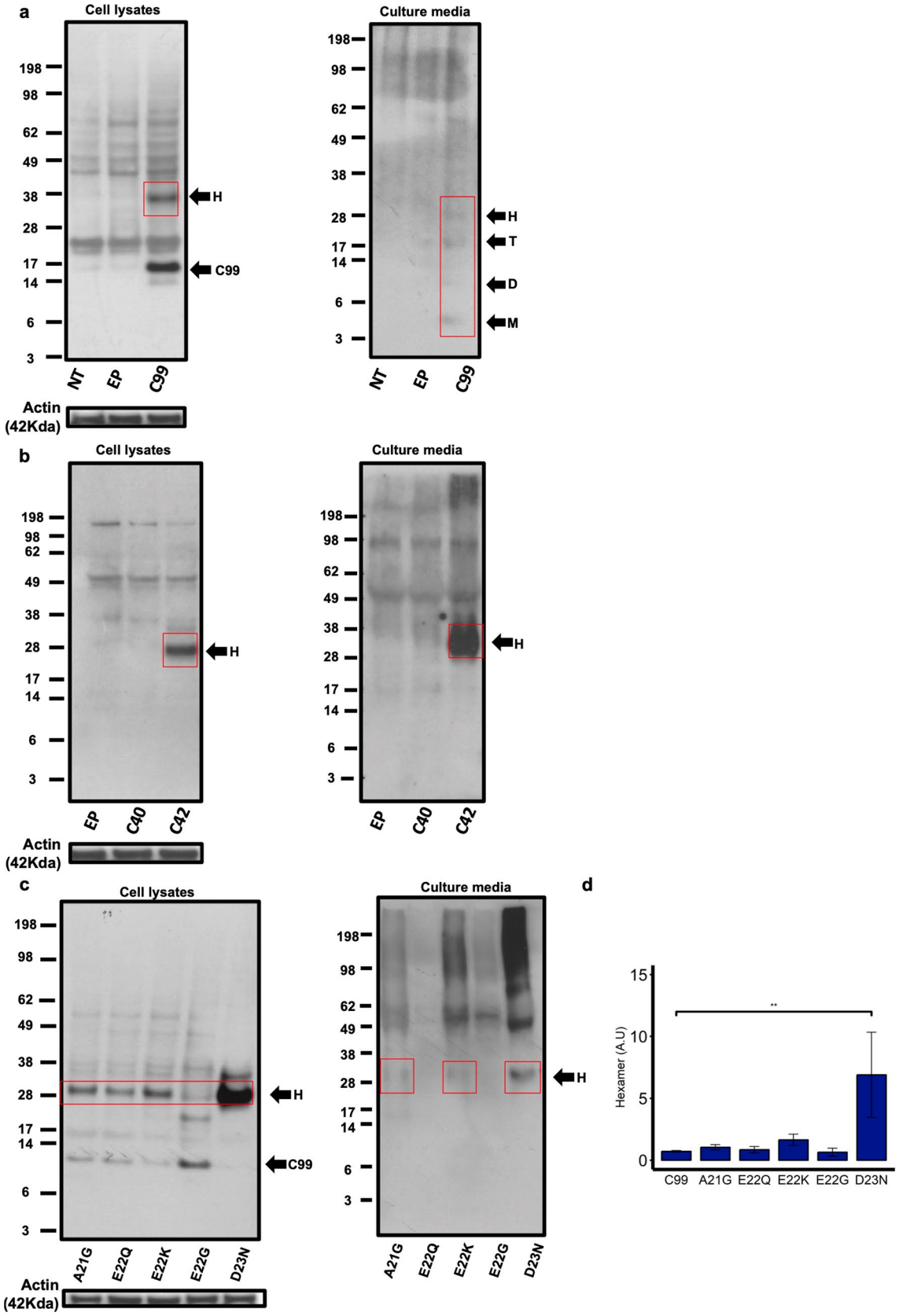
a
Cell lysates
198
98
62
49
38
28
17
14
6
3
H
C99
NT
EP
C99
Actin
(42Kda)
Culture media
198
98
62
49
38
28
17
14
6
3
H
T
D
M
NT
EP
C99
b
Cell lysates
198
98
62
49
38
28
17
14
6
3
H
EP
C40
C42
Actin
(42Kda)
Culture media
198
98
62
49
38
28
17
14
6
3
H
EP
C40
C42
c
Cell lysates
198
98
62
49
38
28
17
14
6
3
H
C99
A21G
E22Q
E22K
E22G
D23N
Actin
(42Kda)
Culture media
198
98
62
49
38
28
17
14
6
3
H
A21G
E22Q
E22K
E22G
D23N
d
Hexamer (A.U)
15
10
5
0
**
C99
A21G
E22Q
E22K
E22G
D23N

◂**Figure 1.** Aβ profile in transfected CHO cells detected with the anti-Aβ W0-2 antibody. (**a**, left panel) Hexamer formation is seen in cell lysates of CHO cells transfected with C99. (**a**, right panel) Monomers (M), Dimers (D), Trimers (T) and Hexamers (H), were detected in the culture media of C99 transfected CHO cells. (**b**, left panel) No assemblies were detected in the cell lysates of C40 transfected CHO cells, however, hexameric Aβ was detected in cell lysates of C42 transfected CHO cells. (**b**, right panel) Hexameric Aβ is also detected in culture media of CHO cells transfected with C42 only. (**c**) Hexameric Aβ is detected in cell lysates and media of CHO cells transfected with FAD mutations in the C99 sequence. Actin (42 kDa) loading controls are provided for the cell lysate conditions. (**d**) Hexamer formation was quantified on the C99 signal (black arrow) for each of the mutations. The D23N (Iowa) mutation showed a significant increase in hexamer formation (**) compared to C99. One-way ANOVA with Tukey's post hoc comparison where $p = < 0.01$ (*), < 0.001 (**), < 0 (***). Error bars are expressed as ± SEM (N = 3). Images of full-length gels are presented in Supplemental Figures S8, S9, S10 for samples presented in Figure 1 only.

compelling argument that the hexamer is the basic building block for the formation of toxic oligomers[15,29]. The majority of these studies investigating the role of hexameric Aβ42 as a nucleus for self-assembly make use of synthetic peptides which are greatly advantageous due to being readily available at high concentrations necessary for biophysical and structural characterisation. However, the true cellular environment and processing of C99 to release Aβ cannot be mimicked using these synthetic peptides.

Furthermore, familial AD (FAD) causing mutations within the Aβ sequence, which are also in the extracellular domain of the C99 sequence, have been shown to have a higher aggregation propensity in previous studies using synthetic and recombinant proteins[30–38]. It is not yet understood whether these FAD mutations which promote self-assembly, increase overall Aβ production, and/or change biochemical properties, also promote/enhance the formation of hexameric Aβ assemblies.

Here, by transfection of Chinese Hamster Ovarian (CHO) cells, we identify the formation of hexamers in Aβ enriched conditions. We also identify for the first time, the formation of hexameric Aβ in CHO transfected with the Flemish (A21G), Dutch (E22Q), Italian (E22K), Arctic (E22G) and Iowa (D23N) FAD causing mutations[39–42]. We have isolated cell-derived hexameric Aβ assemblies and assessed their composition, self-assembly propensity and potential nucleating properties using complementary techniques including Mass Spectroscopy, Thioflavin T (ThT) fluorescence and immunoblotting. We identify these cell-derived Aβ hexamers as Aβ42 assemblies which are likely contributing nuclei for the self-assembly of Aβ monomers. This effect is much more pronounced on monomeric Aβ42 than Aβ40 and is highly dependent on the concentration of available monomers. Furthermore, we show for the first time in a cellular context that the formation of this hexamer is an inherent property of the Aβ42 peptide and its self-assembly propensity, as a self-assembly impaired primary sequence variant of Aβ42 does not form hexamers. The identification of assemblies nucleating Aβ self-assembly in this way provides potential therapeutic targets to prevent oligomer-induced neurotoxicity.

Results

Aβ assembly profile in CHO cells: identification of hexameric Aβ. Although Aβ self-assembly has been extensively studied with synthetic peptides, less is known about the assembly of Aβ peptides produced in a cellular context. As C99 processing precedes Aβ release in physiology, we first assessed the Aβ assembly profile in CHO cells transfected with the human C99 sequence affixed with the signal peptide of the full-length APP in a pSVK3 plasmid backbone. Cell lysates and media of CHO cells were harvested 48 h after transfection and the Aβ profile was assessed by western blotting and detected using the monoclonal human specific anti-Aβ W0-2 antibody (Fig. 1a). In line with what has previously been shown by our group, we confirm that cells transfected with C99 produce a detectable band corresponding to an Aβ assembly size of ~ 28 kDa; the theoretical size of an Aβ42 hexamer[43]. Detection with the anti-Cter antibody against the C-terminal of APP did not identify these bands, consolidating these assemblies are likely to be Aβ and do not contain the CTF of C99 (Supplemental Figure S1). Furthermore, as the band was not detected in the Empty Plasmid (EP) condition, we are confident that the hexamer is not a product of the transfection protocol. Whilst only Aβ hexamers were detected in the cell lysates of these cells, monomers, dimers, trimers and hexamers were detected in the media confirming that in our cellular model, C99 is cleaved to release Aβ detectable both intra- and extracellularly (Fig. 1a). Additionally, we also assessed the Aβ profile of cells transfected with the Aβ40 and Aβ42 sequences affixed with the APP signal peptide (referred to as C40 and C42 respectively), to understand whether the formation of this hexamer in a cellular context was related to one or both of these Aβ isoforms (Fig. 1b). We do not identify a hexameric band in the cell lysates or culture media of C40 transfected CHO cells, which would be ~ 26 kDa in size, in line with the preferential formation of hexamers by Aβ42 previously shown with synthetic peptides[23]. The identification of a hexameric band both intra- and extracellularly in C42 transfected CHO cells suggests that (1) formation of hexameric Aβ is irrespective of whether there is first the processing of the C99 fragment and (2) cell-derived hexamer formation is likely to be an intrinsic property of the Aβ42 sequence itself, as has been demonstrated previously with synthetic peptides[23,26,27]. Finally, as pentamers/hexamers have been suggested to be artifacts of SDS[44], we confirmed the presence of detectable Aβ hexamers in synthetic Aβ42 preparations as well as cell lysates and culture media of C42 transfected CHO cells in native conditions. The samples were harvested and analysed by western blotting in SDS-free conditions and detected with the W0-2 antibody (Supplemental Figure S2a). The same band was not detected by the anti-Cter antibody for cell lysates and culture media samples, as well as synthetic Aβ preparations (Supplemental Figure S2b). Importantly, this enforces our hypothesis that the Aβ hexamer is a relevant oligomeric assembly and not an artifact of experimental conditions.

To link the formation of hexameric Aβ assembly to disease related conditions, we investigated the Aβ profile in CHO cells transfected with the C99 sequence containing the A21G, E22Q, E22K, E22G and D23N FAD

mutations. In Fig. 1c (left panel), we show that in CHO cells transfected with the C99 sequence containing these mutations, there is the detection of hexameric Aβ in cell lysates. The hexamer is also detected in the media of A21G, E22K and D23N expressing cells (Fig. 1c, right panel). In particular, the D23N mutation shows a much more pronounced hexamer formation compared to any other mutant. This was confirmed by quantification of hexamer production in cell lysates normalised to the C99 signal (Fig. 1d) which shows that the D23N mutant generates significantly more hexameric Aβ than the wild-type C99 ($p = < 0.001$), while all other mutants displayed similar levels of hexamer formation. Together, this demonstrates for the first time that hexameric Aβ is occurring in several AD-related conditions.

From these results, we can conclude that the formation of a hexameric assembly is a common feature in Aβ enriched conditions as well as in AD related Aβ mutations where amyloid formation is accelerated.

Isolation and composition of cell-derived Aβ. As the aim of this study was to characterise the formation, self-assembly and possible nucleating properties of the hexamer, we next optimised the isolation of media derived hexameric Aβ. We have focussed here on Aβ material in the media as we hypothesise that the self-assembly leading to the deposition of extracellular amyloid plaques is likely dependent on the presence of this hexamer in the extracellular space. To isolate the Aβ hexamer, CHO cells were transfected with C42 or C99 for 48 h and media was immunoprecipitated using the W0-2 antibody. This was then separated using the Gel Eluted Liquid Fraction Entrapment Electrophoresis (GELFrEE) 8100 system. Briefly, as with SDS-PAGE, this system separates the peptide by size with the added advantage of collecting the assembly size of interest as a liquid fraction. Shown in Fig. 2a, we confirm by western blotting the isolation of hexameric Aβ from the media of CHO cells transfected with C42 and C99 in fraction 5 only (C42 fraction 1–4 shown in Supplemental Figure S3). By isolating and characterising hexamers from both conditions, we are able to assess whether processing affects the self-assembly and nucleating properties of Aβ hexamers. We are also able to isolate C99-derived Aβ monomers in fraction 1, however, as lower molecular weight assemblies were not detectable in CHO cells transfected with C42, even when samples were harvested at earlier time points (Supplemental Figure S4), this was not possible for C42 transfected CHO cells. Considering the highly hydrophobic and aggregation prone nature of the Aβ42 sequence, it is unsurprising that we cannot detect lower molecular weight assemblies which, if present, are likely too low in concentration to detect by western blotting.

To identify the isoform of Aβ in the C42 and C99-derived hexameric assemblies, we carried out dot blotting using anti-Aβ42 and anti-Aβ40 specific antibodies (Fig. 2b) with synthetic preparations of Aβ40 and Aβ42 as positive controls. Dot blotting with W0-2 (Fig. 2b, left panel) antibody was used to confirm the presence of the proteins. Our results clearly show the Aβ42 specific antibody binds to hexameric assemblies from both conditions (Fig. 2b, right panel), although the signal for the C99- derived hexamer is less prominent. Importantly, no signal is seen for either hexamer with the Aβ40 specific antibody (Fig. 2b, middle panel), thus confirming the Aβ hexamers are Aβ42 assemblies. A dot blot with the anti-Cter antibody (Supplemental Figure S3) confirms that the isolated hexamers from C42 and C99 transfected CHO cells do not contain the CTF of APP.

The formation of a hexameric assembly is an inherent property of the Aβ42 peptide due to self-assembly propensity. The preferential formation of hexameric Aβ has been suggested to be linked to the C-terminus of Aβ42 and its self-assembly propensity[23]. To assess this in our cellular model, CHO cells were transfected with an assembly-impaired variant of the C42 sequence, vC42, and the Aβ profile was assessed by western blotting and detection with the W0-2 antibody (full primary sequence can be found in Supplemental Table S1). This is the same sequence that has been previously reported and thoroughly characterised as being self-assembly impaired despite only a two amino acid difference (F19S and G37D) compared to the wild-type Aβ42 sequence[45]. Figure 3 demonstrates that CHO cells transfected with this variant produced only dimers and trimers in the cell lysates and no detectable assemblies in the media. The lack of a hexameric assembly confirms the importance of self-assembly in the formation of this structure and its direct link to Aβ42 aggregation propensity.

Cell-derived Aβ42 hexamer formation is a direct consequence of Aβ42 primary sequence. As both monomeric and hexameric Aβ were detected and isolated from C99 transfected cells, we next questioned whether the C99-derived Aβ monomers isolated in Fraction 1 (Fig. 2a) were able to assemble into hexamers. No assembly of the isolated Aβ monomers was seen by western blotting over 48 h, the time in which we see hexamer presence in the cell lysates and media of C42 and C99 transfected CHO cells (Fig. 4a). Electro-chemiluminescence immunoassay (ECLIA) measurements, which provide quantitative analysis of monomeric Aβ, were performed on the media of C99 transfected CHO cells (Fig. 4b) before immunoprecipitation for Aβ and confirmed that Aβ40 was in high abundance (80.9 pg/mL) whereas very low concentrations of Aβ42 (1.3 pg/mL) were detected. This provided early indications that the monomer detected by western blot (Fig. 1a) is likely to be Aβ40. Analysis of the isolated monomer fraction by mass spectrometry (Fig. 4c) revealed that, in line with the reduced self-assembly properties reported in the literature[46], only the Aβ40 sequence was identified in this sample. Finally, we have confirmed by western blotting that Aβ40 is unable to form hexamers even in a cellular context, as CHO cells transfected with C40 do not produce a detectable band for this assembly in either cell lysates or media (Fig. 1b). qPCR data consolidated that this was not due to low transfection efficiency (Supplemental S5).

Together, these data show for the first time from cell-derived material that Aβ40 does not readily form hexameric assemblies, which in turn reinforces that the primary sequence of Aβ42 and its resultant self-assembly properties are determining factors in the formation of a hexameric assembly.

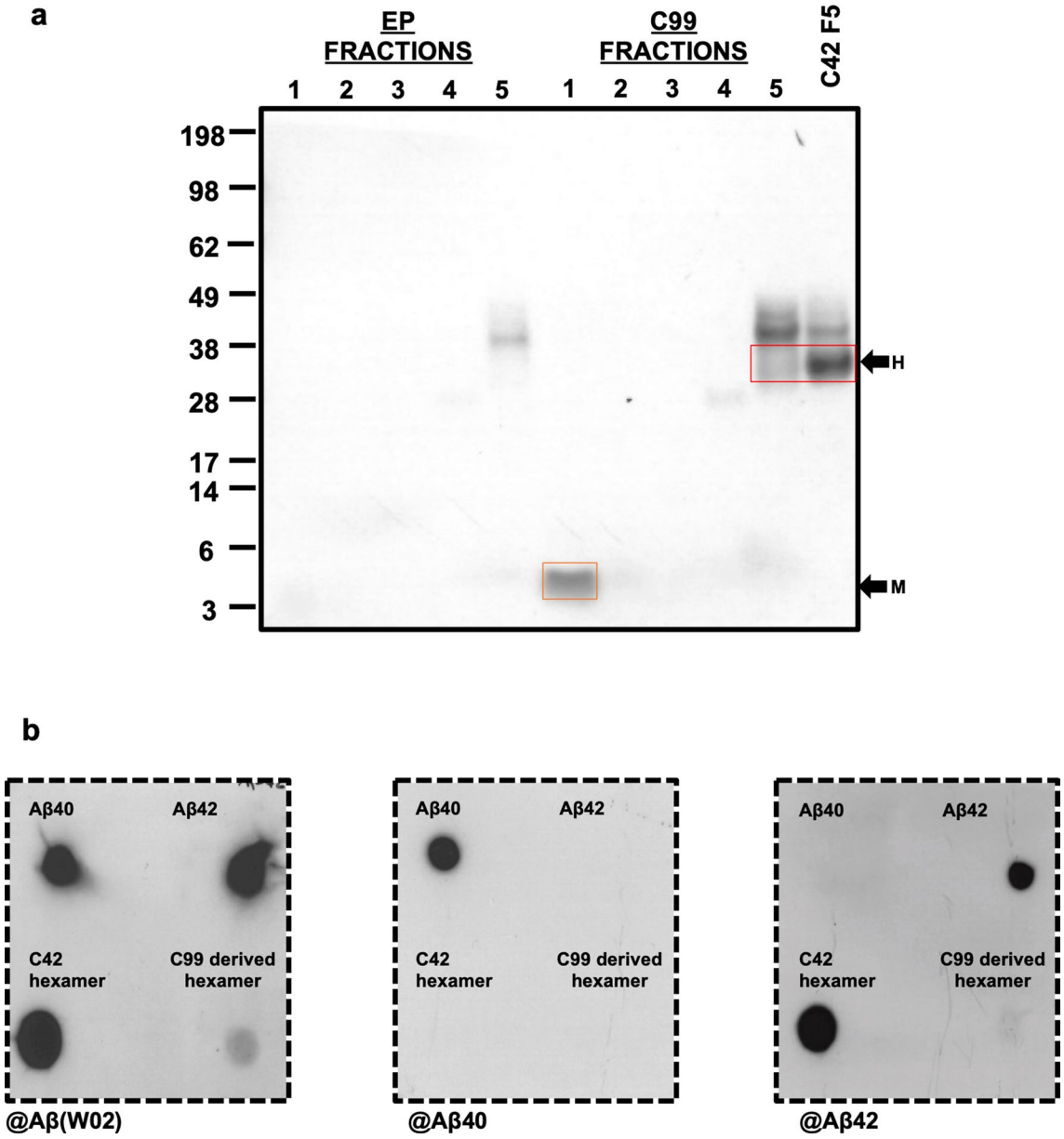

Figure 2. Isolation of Aβ assemblies and identification of hexameric assembly Aβ isoform. (**a**) Aβ was immunoprecipitated using the W0-2 antibody and separated by size using the GELFrEE 8100 system. CHO cells transfected with the empty plasmid (EP) and immunoprecipitated for Aβ did not show isolated assemblies in any fraction. From C99 transfected CHO cells, we are able to isolate monomeric Aβ (orange box) in Fraction 1 and hexameric Aβ (red box) in Fraction 5 (F5). Only hexameric Aβ was isolated (Fraction 5) from C42 transfected CHO cells. (**b**) Dot blotting was carried out to identify the hexameric Aβ isoform using the W0-2, anti-Aβ40 and anti-Aβ42 antibodies. Synthetic Aβ40 and Aβ42 were used as positive controls. Both C42 and C99 derived Aβ hexamers are detected by the anti-Aβ W0-2 antibody (left panel) and anti-Aβ42 antibody (right panel), however, not by the anti-Aβ40 antibody (middle panel) confirming the hexamers are composed of Aβ42. Dashed border indicates the membrane was cut before detection.

Isolated hexameric Aβ42 does not self-assemble into higher molecular weight assemblies. In order to establish the self-assembly properties of the isolated hexameric Aβ42 derived from media of C42 and C99 transfected CHO cells (Fraction 5 shown in Fig. 2a), we first carried out a ThT fluorescence assay as a measure of fibril formation. 150 μM of hexameric Aβ was incubated with 20 μM ThT and fluorescence was monitored over 48 h. Figure 5a shows that over this time course, there is no increase in fluorescence seen which suggests that the hexameric assembly does not form fibrils in the timeframe of our experiment. To further consolidate this and detect any pre-fibrillar assemblies that may not bind to the ThT dye, western blotting was carried out on the same samples at several time points (Fig. 5b and c). Detected by the W0-2 antibody, we see there are no higher molecular weight assemblies at longer time points and only the hexameric assembly is detected for C42-derived hexamers. This also confirms that there is no degradation or disassembly of the peptide. However,

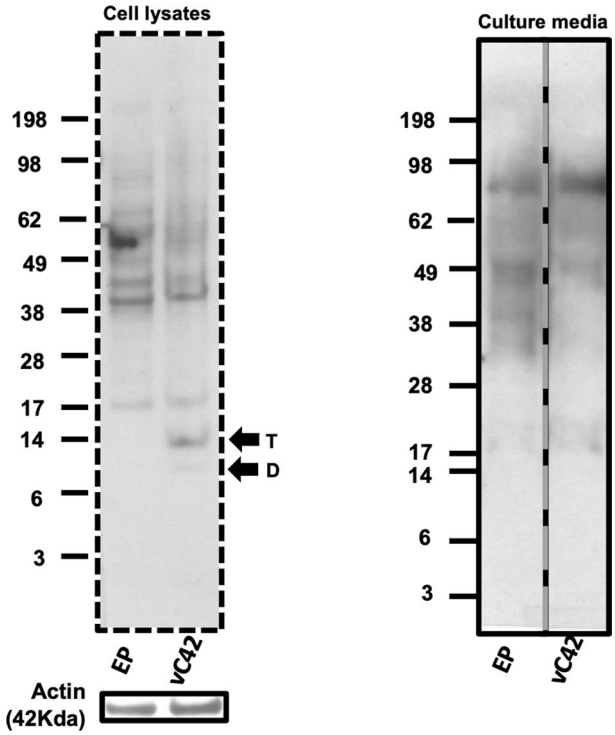

Figure 3. Hexamer formation is directly related to Aβ42 self-assembly propensity. CHO cells transfected with vC42 (F19S, G37D), did not form hexameric Aβ in either the cell lysates or media detected by the W0-2 antibody. However, dimers (D) and trimers (T) were detected in the cell lysates of vC42 transfected CHO cells. Actin (42 kDa) loading controls are provided for the cell lysates conditions. Vertical dashed lines indicate that samples were run on the same gel, but lanes are not contiguous. Dashed border indicates the membrane was cut before detection. A full-length gel image of the media samples is presented in Supplemental Figure S11.

although C99-derived Aβ42 hexamers do not assemble into higher molecular weight assemblies, monomers are detected with increasing intensities over time. This suggests that in the C99 transfected conditions where processing is taking place, the hexamer is less stable and does disassemble into monomers. This is reflective of the dynamic nature of self-assembly, particularly in the formation of a critical nucleus. As we have identified the hexamers to be only composed of the Aβ42 isoform, these data also allow us to conclude that the monomers detected from the disassembled C99-derived hexamers are likely to be Aβ42 monomers. Combined, these data show no further self-assembly of hexameric Aβ assemblies derived from both C42 and C99 in our experimental conditions. We therefore conclude that these cell-derived hexameric assemblies have similar self-assembly properties in our experimental conditions; the hexamer on its own does not self-assemble into higher molecular weight assemblies, however, the stability of C99-derived Aβ42 hexamers is weaker than that of C42-derived Aβ42 hexamers.

Hexameric Aβ42 enhances self-assembly of Aβ42 in the early stages of aggregation. Finally, we assessed the effect of Aβ42 hexamer addition on monomeric synthetic Aβ42 (mAβ42) aggregation with increasing amounts of isolated C42 and C99-derived Aβ42 hexamers (Fig. 6a). Aβ42 was prepared as previously described[45] using a protocol that has been shown to be predominantly monomeric immediately after preparation and diluted to a working stock concentration of 50 μM. ThT fluorescence of mAβ42 without any seeding (Supplemental Figure S6a) shows a low ThT fluorescence between 0–4 h. Based on the previous characterisation of Aβ42 self-assembly using this preparation method[45,47], we believe this early timeframe reflects the lag phase of aggregation. Between 4–16 h, there is a steep increase in ThT fluorescence which likely represents the elongation phase, as has been previously shown, and a plateau is reached after 16 h[45,47,48]. We show this aggregation to be concentration dependent in Supplemental S6b and used this data to decide upon 50 μM as our working concentration to carry out seeding experiments within a reasonable timeframe. The concentration of hexamer used for seeding was a percentage of the mAβ42 concentration and the final solution was incubated with 20 μM ThT dye. As the hypothesised nucleating effects of the hexamer are expected to be in the early stages of assembly, ThT fluorescence was monitored for 4 h and normalised for each condition to itself at T0 as a representation of increased fluorescence at each time point (Fig. 6a).

The addition of 5% (light pink line) and 10% (dark pink line) C42-derived hexamer immediately results in an increase in fluorescence intensity, as does the addition of 5% (light green line) C99-derived Aβ42 hexamer. This suggests increased self-assembly kinetics in the early stages of aggregation for these conditions, however, 10% (dark green line) addition of C99-derived Aβ42 hexamer results in a similar ThT fluorescence as mAβ42 alone

(black line). This aggregation enhancing effect of the hexamers, particularly in the early time points, is shown with more clarity in Supplemental Figure S6c with additional data points between T0-4 h. Complementary to the ThT aggregation assay, we assessed the range of assembly sizes present at T0 and 2 h after hexamer addition by western blotting using the W0-2 antibody (Fig. 6c). By 2 h, both seeded conditions show the formation of a larger range of higher molecular weight assemblies which migrate as a smear, as well as bands detected in the well of the gel. As the detection of this band in the well is concomitant with the increase in ThT fluorescence, we believe that this band is likely to be fibrils 'stuck' in the well of the gel, however, electron microscopy is needed to confirm the presence of these fibrils. mAβ42 without seeding displays bands corresponding to monomers, dimers and trimers only. Western blotting for mAβ42 seeded with C99-derived Aβ42 hexamers (Fig. 6c) also revealed similar trends to that of C42-derived hexamer seeding where higher molecular weight assemblies were detected at T0 in the seeded conditions, and by 2 h, what likely corresponds to fibrils were 'stuck' in the wells of the gel. As we have identified both hexamers to be Aβ42, this is unsurprising. Interestingly, in contrast to what was seen with the ThT fluorescence, 10% addition of C99-derived Aβ42 hexamers does result in the formation of higher molecular weight assemblies by 2 h, perhaps suggesting the formation of ThT negative aggregates. Combined, the increase in ThT fluorescence seen in the seeded conditions, compared to non-seeded mAβ42 only, supports the hypothesis of the hexamer as a nucleus for self-assembly.

Although our ThT assay is representative of qualitative analysis and is not suitable for quantitative kinetic analysis, we have calculated the gradient of the graph for each condition from 0–1 h for a numerical indication of effects on the early stages of aggregation (Fig. 6d). This analysis is to further consolidate the conclusion that Aβ42 hexamer addition enhances self-assembly in the early stages of aggregation, however, interpretations cannot be made regarding the kinetics and microscopic steps of aggregation e.g., primary and secondary nucleation. The addition of 5% C42 and C99-derived hexamer significantly increases the gradient of the graph (0.51 AU ± 0.03 SEM, 0.4AU ± 0.05 SEM respectively, $p = < 0.01$) compared to mAβ42 alone (0.16 AU ± 0.05 SEM). Although an increase was also seen with 10% C42 hexamer (0.32 AU ± 0.1 SEM), this was not significant. This is likely due to the fact that the nucleating potential of the cell-derived C42 hexamer is dependent on the available monomers in solution. Furthermore, the same increase in early assembly kinetics was not seen with 10% C99-derived Aβ42 seeding (0.1 AU ± 0.06 SEM). This might be due to the difference in stability of the C99-derived Aβ hexamer; as it disassembles into monomers with time (Fig. 4c), the concentration of monomers continues to dominate the solution population and there is perhaps not enough hexamer in solution to nucleate self-assembly, which indicates a threshold concentration is required before nucleating effects can be seen.

Finally, we also assessed the effects of both hexamers on monomeric Aβ40 (mAβ40) prepared using the same protocol as for mAβ42 (Fig. 7). Firstly, in non-seeded conditions, we show a reduced aggregation of 50 μM Aβ40 compared to 50 μM Aβ42 in Supplemental Figure S6a, however we confirm that Aβ40 aggregation does occur across a range of concentrations in Supplemental Figure S6d. In seeded conditions, no increase in slope gradient at early time points (0–1 h) was seen for mAβ40 seeded with 5% and 10% C42 or C99-derived Aβ42 hexamers respectively. The lack of self-assembly enhancing effects at early stages of aggregation was further consolidated by western blotting (Fig. 7c) which revealed assembly sizes ranging from monomers to tetramers only for all conditions at T0 and 2 h, and no increase in higher molecular weight species. The ThT fluorescence for both 5 and 10% C42-derived hexamer seeding does begin to slightly increase after 4 h which could be indicative of a reduced ability of these hexamers to nucleate Aβ40 compared to Aβ42. A similar and more pronounced trend of increased ThT fluorescence is seen with 5 and 10% C99-derived Aβ hexamers from 2 h onwards. Interestingly, as the increase in fluorescence was not seen in mAβ42 seeded with 10% C42-derived hexamers (Fig. 6) and as we have shown the C99-derived hexamers to disassemble into monomers, this data suggests some effect of two monomeric Aβ isoforms interacting.

Together, we conclude that the cell-derived Aβ42 hexamers have a reduced aggregation enhancing effect on Aβ40 which further reiterates the direct link of hexamers as likely critical nuclei for Aβ42 self-assembly. To be sure of this reduced capacity as opposed to inability, we seeded mAβ40 with 30% C42 and C99-derived hexamers (Supplemental Figure S7), which confirms that with enough hexamer, seeding can occur.

Our data demonstrate for the first time, the ability of cell-derived Aβ42 hexamers to enhance self-assembly in early stages of aggregation with preferential nucleation of monomeric Aβ42 compared to Aβ40.

Discussion

The process of self-assembly and its importance in Aβ toxicity has been the focus of several research studies. The formation of intermediary oligomeric species during this process has been identified as being a determinant of cytotoxicity and we therefore investigated an Aβ assembly that is hypothesised to be responsible for facilitating nucleation dependent amyloid formation. To the best of our knowledge, we are the first group to present a thorough characterisation of cell-derived hexameric Aβ and provide more physiologically relevant evidence than in vitro studies using synthetic or recombinant peptides, to further support this assembly to be a nucleation enhancing entity.

The identification of specific Aβ intermediate assemblies that serve as nuclei for fibril formation has remained elusive due to their transient and heterogenous nature. Despite this, several studies have optimised the use of highly sensitive techniques such as small angle neutron scattering (SANS), small angle X-ray scattering (SAX) and sedimentation velocity (SV) analysis complementary to SDS-PAGE of photo-induced cross linking of unmodified proteins (PICUP) solutions of Aβ to detect hexameric assemblies involved in the early stages of self-assembly[26–28]. Furthermore, a recent native ion mobility-mass spectrometry study has also identified the formation of hexameric Aβ and suggests a β-barrel structure in membrane mimicking environments[49]. In line with our data, these studies have all consistently observed the formation of hexameric Aβ to be highly prone to the Aβ42 sequence. However, these studies have relied heavily on synthetic peptides which cannot mimic a cellular environment.

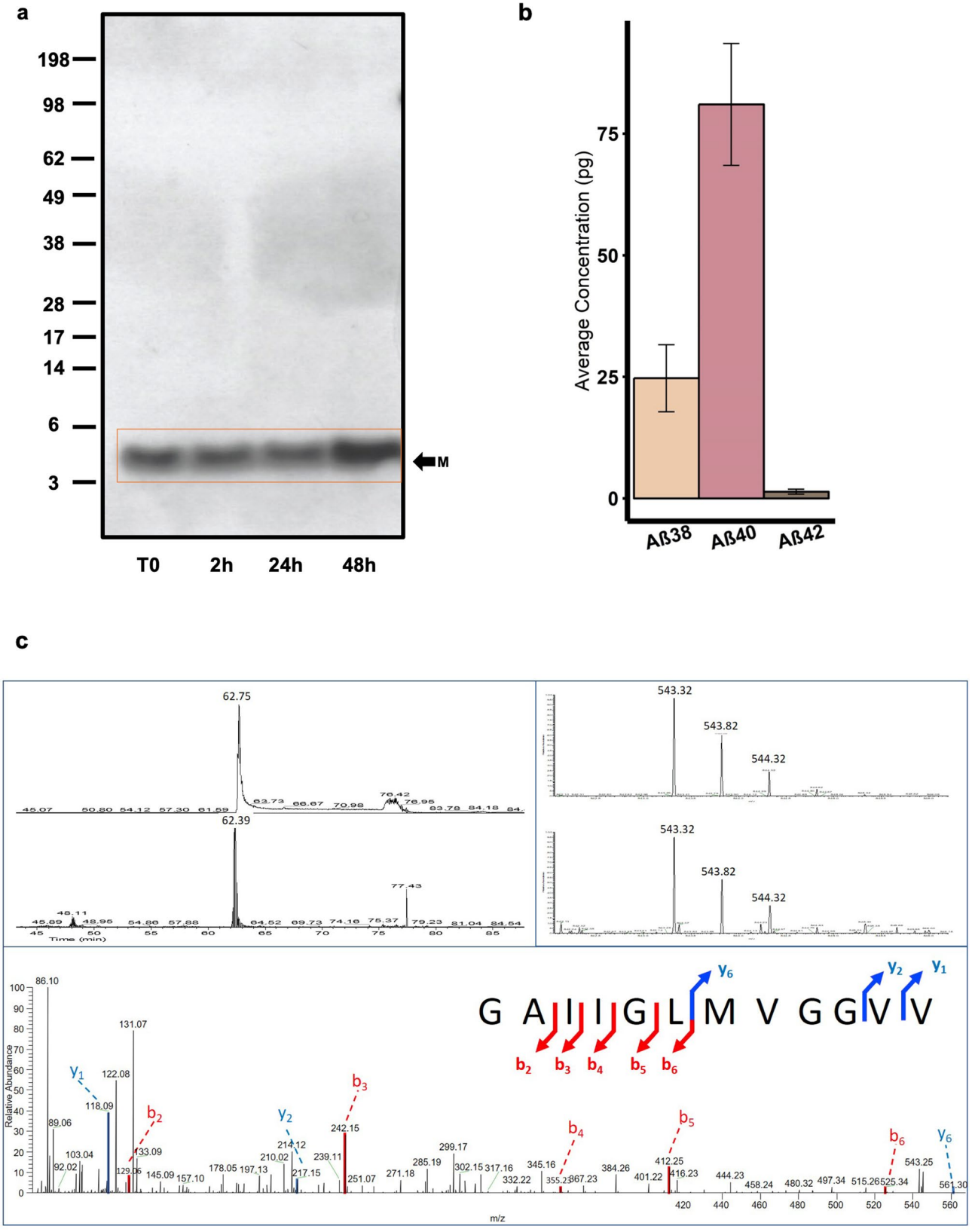
a
198
98
62
49
38
28
17
14
6
3
M
T0
2h
24h
48h
b
Average Concentration (pg)
75
50
25
0
Aß38
Aß40
Aß42
c
62.75
62.39
77.43
Time (min)
543.32
543.82
544.32
543.32
543.82
544.32
Relative Abundance
m/z
G A I I G L M V G G V V
b2 b3 b4 b5 b6
y6 y2 y1

◂**Figure 4.** Hexamer formation is directly related to Aβ42 primary sequence. (**a**) Isolated monomeric Aβ incubated at room temperature over 48 h does not assemble into hexameric or other higher molecular weight assemblies as assessed by western blotting detected with the W0-2 antibody. A full-length gel image is presented in Supplemental Figure S12. (**b**) ECLIA measurements (N = 5) on the media of C99 transfected CHO cells identified Aβ40 as the most abundant monomeric Aβ isoform (80.9 pg/ml). Low concentrations of Aβ38 (24.7 pg/ml) and even lower concentrations of Aβ42 (1.3 pg/ml) were detected in this culture media (**c**) CLC-MS/MS identification of Aβ40 in the C99 Sample. Top left panel: extracted ion chromatogram of the [M + 2H]2 + detected at 62 min, for the standard (top) and the C99 sample (bottom). Top right Panel: mass spectra of the Aβ40 fragment ion showing the isotopic pattern for the standard (top) and the C99 sample (bottom). Bottom panel: MS/MS annotated spectrum characterising an Aβ40 fragment from the C99 sample.

Here, in our experimental conditions, we have identified a non-self-assembling Aβ42 specific hexamer that is present in both the cell lysates and media of transfected CHO cells.

CHO cells transfected with either C99 or C42 sequences showed the ability to form an Aβ assembly that was ~ 28 kDa in size by western blotting, which is the theoretical size of an Aβ42 hexamer. FAD Aβ mutations in the C99 sequence also showed the formation of hexameric Aβ in the cell lysates and media of CHO cells suggesting that the formation of this assembly is common in Aβ enriched and FAD related conditions. The commonality of hexameric Aβ across these conditions highlights for the first time in a more physiological context, the importance of this assembly in conditions where Aβ self-assembly is accelerated.

Dot blotting following the isolation of these hexamers from the media of C42 and C99 transfected cells, confirmed them to be Aβ42 assemblies. On the contrary, the monomeric Aβ identified and isolated from the media of C99 transfected CHO cells was confirmed to be composed of the Aβ40 sequence only. Furthermore, this monomer did not assemble into hexamers or any other higher molecular weight assemblies in the parameters of our experiments. This information is important as it confirms that the ability to readily form a hexameric assembly in a cellular context is an inherent property of the Aβ42 primary sequence. This was further supported by the lack of a hexameric assembly seen in the cell lysates and media of CHO cells transfected with the vC42 sequence which has both F19S and G37D substitutions. These substitutions have been shown to negatively affect self-assembly propensity[35,50–56]. In this way, vC42 also begins to provide some evidence to suggest that both the F19 and G37 amino acids are important residues in the formation of a hexameric assembly. Interestingly, whilst this peptide was shown to remain largely monomeric for 7 days in vitro[45] we show here in cellular context, the formation of dimers and trimers within 48 h. This further highlights the physiological relevance of our study in which we show the importance of protein translation, the cellular environment and the subsequent Aβ42 assemblies formed.

Our data strongly supports the conclusion that the Aβ hexamers we have identified are Aβ42 specific assemblies. This, combined with the assumption that there are no other isoforms present in the C42 condition, as well as C99-derived hexameric Aβ disassembling back into monomers over time, suggests the initial nascent Aβ42 monomer may be responsible for the formation of the Aβ42 hexameric structures identified here. A previous study exploring the decapeptide Aβ (21–30) showed its protease resistance was identical to full length of Aβ42 and likely to organise intramolecular monomer folding and therefore an initial folding nucleus[57]. This has been attributed to a β-turn formed and stabilised by both hydrophobic and electrostatic interactions between V24-K28 and K28-E22/D23. FAD related mutations at positions G22 or D23 therefore disrupt this turn stability and have been shown to enhance subsequent assembly and oligomerisation[55,58,59]. The level of turn disruption correlates directly with enhanced oligomerisation for each mutation; from our results, the D23N mutation significantly disrupts the turn stability and enhances the formation of hexameric Aβ42. The importance of this monomer folding nucleus in the formation of higher molecular weight assemblies, such as the hexamer, has been explained by the formation of the stabilised turn being a kinetically favoured folding event capable of facilitating the interaction between the central hydrophobic cluster (L17-A21) and the C-terminus, which is far more pronounced in Aβ42 than in Aβ40[59]. Together, this provides a plausible explanation as to (1) how the hexameric assembly is linked to folding events in the monomeric Aβ42 peptide (2) why FAD mutations explored in this study do not negatively affect hexamer formation[60]. The disruption of the stabilising interactions in the decapeptide region of monomeric Aβ may occur in a physiological environment such an acidic pH (e.g. endosomes) where Aβ assembly is known to be enhanced.

We also show that hexameric assemblies that are formed from Aβ after C99 processing are less stable than those formed from C42 where there is no upstream processing, suggesting processing may have an effect on structural properties. Despite this, both hexamers display nucleating properties which points to size being an important contributor for nucleating potential. Interestingly, hexamers have also been identified as being important intermediates in the self-assembly of β2-microglobulin which suggests this assembly size may play an important role in the aggregation of several amyloid forming proteins[61].

Several oligomeric species that are multimers of a hexameric unit e.g. ADDLs and Aβ*56, which would likely require hexameric self-association, have been identified. However, in the parameters of our experiments, the hexamer does not self-associate to form higher molecular weight assemblies. Hexamers with the ability to self-associate may be in a different conformation and/or require suitable conditions for self-association such as membrane interactions or an acidic environment. Furthermore, the lack of association of two hexamers to form a dodecamer, which is thought to occur due to stacking of two hexamers with their hydrophobic C-terminal ends at the centre of the structure[22] was also observed by Österlund and colleagues. They concluded the reduced entropic drive towards hexamer dimerisation is likely due to the C-termini being stabilised in their experimental conditions which are likely mimicking the effects that would be seen in a lipid bilayer[49]. Therefore, perhaps the

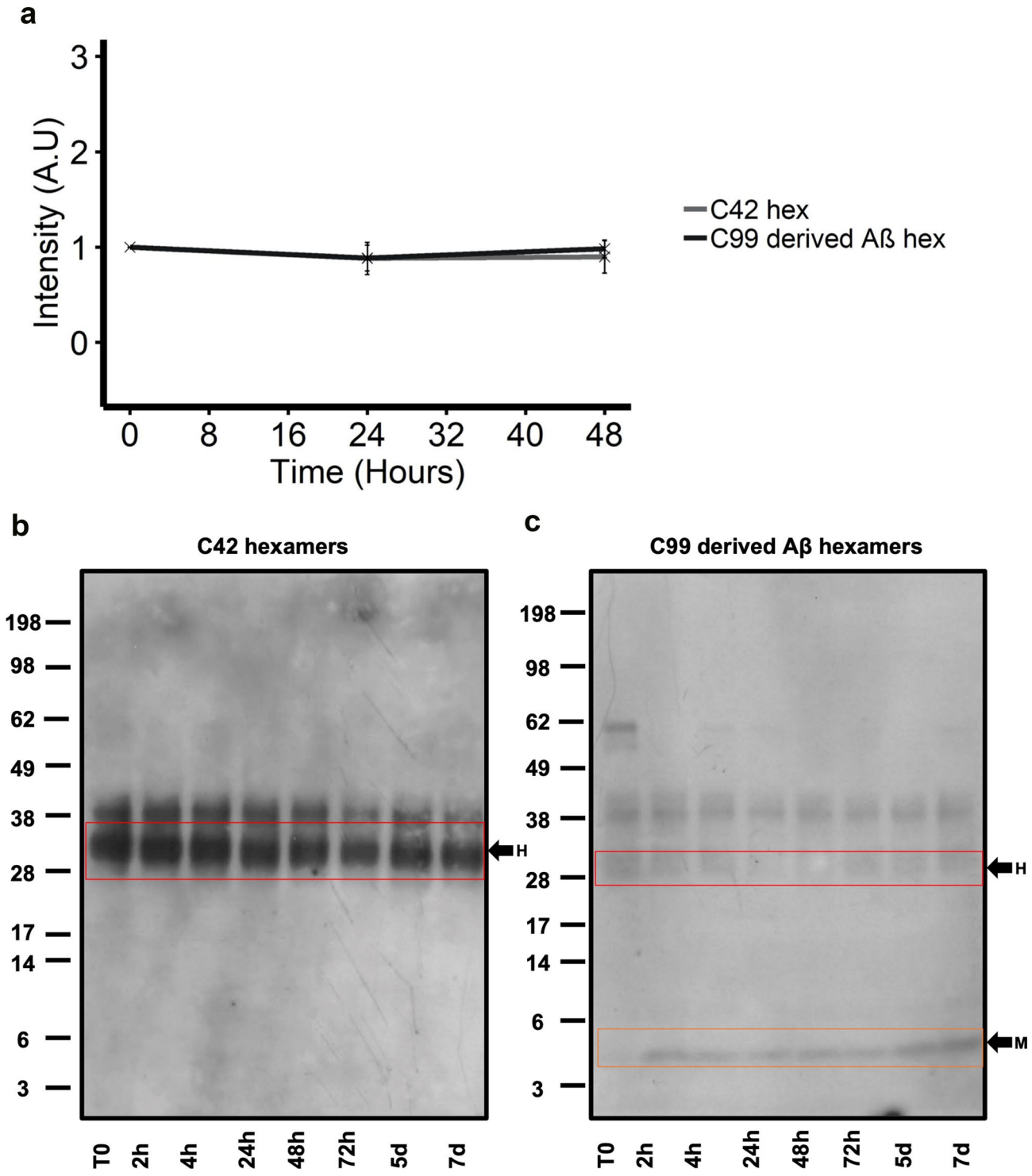

Figure 5. Isolated hexameric Aβ does not self-assemble into higher molecular weight assemblies (**a**) 150 μM isolated hexameric Aβ from C42 and C99 transfected CHO cells was incubated with 20 μM ThT and fluorescence was monitored over 48 h as a measure of fibrillogenesis. No increase in fluorescence was seen for either of the isolated hexamers. (**b** and **c**) Western blotting and detection with the W0-2-antibody revealed both hexamers (red box) do not assemble into higher molecular weight assemblies over 7 days. Hexamers from C99 transfected CHO cells, do, however disassemble into monomers (orange box) over time as was detected from 2 h onwards.

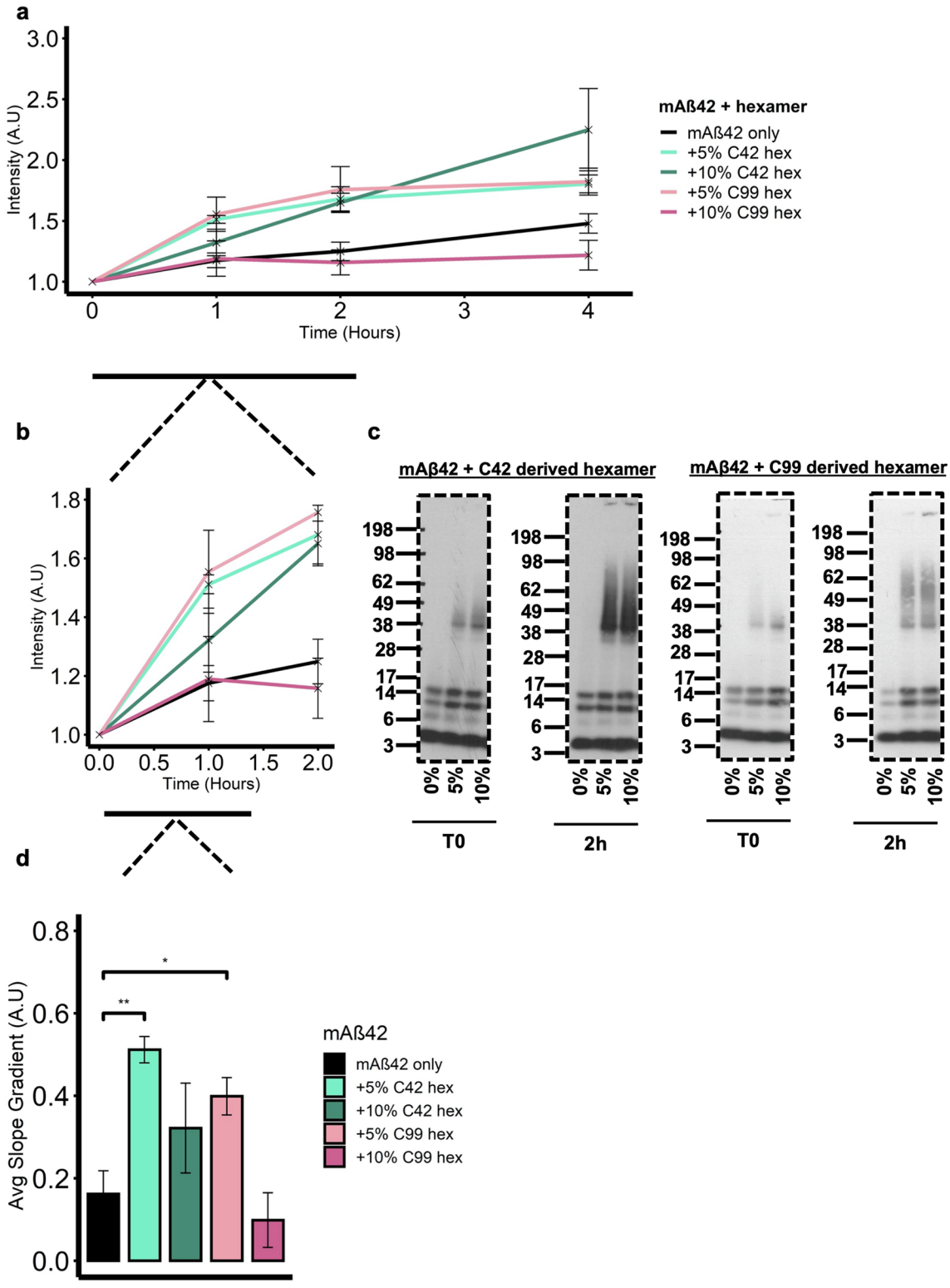

Figure 6. Isolated C42 and C99 derived hexameric Aβ nucleate monomeric Aβ42 (mAβ42). (**a**) 50 µM mAβ42 was seeded with 5- or 10% hexamer and the solution was then incubated with 20 µM ThT. Fluorescence was monitored over 24 h. (**b**) Addition of both 5- and 10% C42 hexamer results in an immediate increase in ThT fluorescence (0–2 h). (**c**) Western blotting with the W0-2 antibody revealed all seeding conditions form higher molecular weight assemblies at T0 and by 2 h what likely correspond to fibrils are seen 'stuck' in the wells of the gel. Dashed borders indicate the membrane was cut before detection. (**d**) The gradient of the ThT fluorescence slope was calculated at the early time points of aggregation (0–1 h) and One-way ANOVA with Tukey's post hoc comparison where $p = < 0.01$ (*), < 0.001 (**), < 0 (***), revealed addition of 5% C42 hexamer significantly (**) increased the kinetics of aggregation compared to mAβ42 only as did the addition of 5% C99 derived hexamer (*). Error bars are expressed as ± SEM.

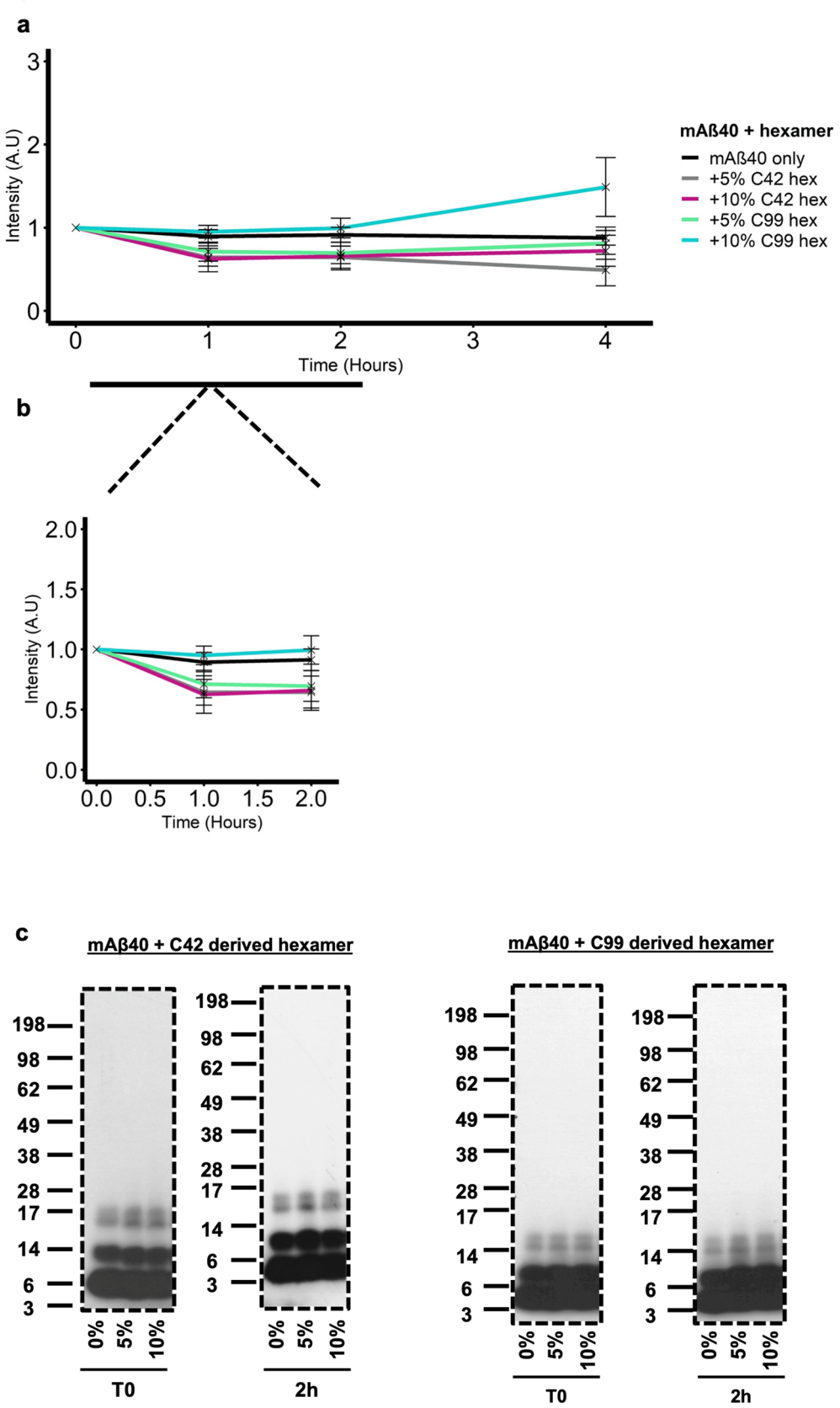

Figure 7. Isolated C42 and C99 derived hexameric Aβ do not readily nucleate monomeric Aβ40 (mAβ40). (**a**) 50 μM mAβ40 was seeded with 5- or 10% hexamer and the solution was then incubated with 20 μM ThT. Fluorescence was monitored over 4 h. (**b**) Addition of both 5- and 10% did not result in an increased fluorescence at early time points (0–2 h) (**c**) Western blotting detected with the W0-2 antibody revealed seeding conditions with both hexamers does not lead to the formation of higher molecular weight assemblies compared to mAβ40 only. Dashed borders indicate the membrane was cut before detection.

hexamers we isolate here are or have been associated to these lipid bilayers which affects their self-association properties.

Importantly, we show for the first time the self-assembly enhancing potential of both C42 and C99 cell-derived hexamers and show this to be preferential to mAβ42 over mAβ40. Based on our data and literature surrounding Aβ hexamers, we believe that this is to be a nucleating effect. This likely nucleation propensity is heavily reliant on the available monomers in solution, in line with the definition of a nucleus for self-assembly during the lag phase of amyloid formation[21].

Overall, we demonstrate for the first time in a cellular context, the formation of hexameric Aβ42 as a common feature in conditions where Aβ42 self-assembly is accelerated and we have characterised these hexamers to be non-self-assembling entities that preferentially nucleate the aggregation of monomeric Aβ42. Understanding mechanisms that can enhance or facilitate self-assembly in this way will ultimately aid our understanding of amyloid pathology.

Materials and methods

Chemicals and reagents. Nitrocellulose membranes were purchased from GE Healthcare (Little Chalfont, UK) and Western Lightning Plus-ECL from PerkinElmer (Waltham, MA, USA). The anti-Aβ W0-2 (MABN10) primary antibody was from Abcam (Cambridge, UK), anti-Aβ40 and anti-Aβ42 primary antibodies were purchased from Merck Millipore (Darmstadt, Germany). The anti-Cter primary antibody and horse radish peroxidase (HRP)-conjugated secondary antibodies were purchased from Sigma-Aldrich (St Louis, MO, USA). TRIzol reagent and Complete protease inhibitor cocktail were from Roche (Basel, Switzerland). The cDNA synthesis kit and iQ SYBR Green Supermix were from Bio-Rad (Hercules, CA, USA).

DNA constructs. The pSVK3 empty plasmid (EP) as well as the -C40, -C42 and -C99 vectors including the fused signal peptide of APP were described previously[43,62]. QuickChange site-specific mutagenesis (Stratagene, La Jolla, CA, USA) was used to produce the FAD mutants in the pSVK3-C99 template DNA, as previously described[63]. Primer sequences can be found in Supplemental Table S2.

Cell culture and transfection. Chinese hamster ovary (CHO) cell lines were cultured in Ham's F-12 medium supplemented with 10% of FBS and 1% Penicillin–Streptomycin (Life Technologies, Carlsbad, CA, USA). All cell cultures were maintained at 37 °C in a humidified atmosphere (5% CO_2). Cells were passed every 4 days at ~ 80% confluency and no longer used after passage 20.

For transfections with C99 and Aβ sequences, approximately 2.2×10^6 CHO cells were plated 24 h in advance in 10 cm petri dishes. A transfection mix of 15 µg of DNA, 30 µl Lipo2000 (Invitrogen) in 1 ml Opti-MEM was incubated for 15 min at room temperature before being added to cells. A 0% FBS medium change was carried out 24 h after transfection and both cells and media were harvested after 48 h of initial transfection.

Western and dot blotting. After transfection, cell lysates were harvested and sonicated in lysis buffer (Tris 125 mM pH 6.8, 4% sodium dodecyl sulfate, 20% glycerol) with Complete protease inhibitor cocktail. Media were centrifuged at 1200 g for 5 min to pellet any debris and dead cells and the supernatants were lyophilised by SpeedVac. For cell lysates, 40 µg of protein were heated for 10 min at 70 °C in loading buffer (lysis buffer supplemented with 50 mM DTT and LDS sample buffer). The lyophilised media were resuspended in 400 µl milli-Q (mQ) water and the maximum sample volume was loaded. Samples were loaded and separated on 4–12% NuPAGEbis-tris gels (Life Technologies), and then transferred for 2 h at 30 V onto 0.1 µm nitrocellulose membranes. After 30 min of blocking (5% non-fat milk in 0.1% PBS-Tween), membranes were incubated at 4 °C overnight with primary antibodies. Membranes were then washed three times in 0.1% PBS-Tween for 10 min and incubated with horse radish peroxidase (HRP)-conjugated secondary antibodies for 1 h at room temperature. Finally, membranes were again washed three times for 10 min in PBS-Tween prior to ECL detection. Membranes were stripped with boiling 1X PBS for 10 min before being re-detected with the anti-Actin antibody. Primary antibodies dilutions for western blotting are as follows: anti-Aβ W0-2 (1:1.500), anti-Cter (1:2.000) and anti-Actin (1:1000). Secondary antibodies dilutions are as follows: anti-mouse (1:10.000) or anti-rabbit (1:10.000). Both primary and secondary antibodies were diluted in 0.1% PBS-Tween.

For dot blotting, 5 µl of sample (150 µM isolated Aβ hexamers, 50 µM synthetic monomeric Aβ) were spotted onto 0.1 µm nitrocellulose membranes. Once the samples were dry, a further 5 µl of sample were spotted twice on top and dried. The membranes were boiled in PBS for 3 min twice and blocked in 5% non-fat milk in PBS-Tween for 30 min. After this the membranes were washed, incubated with antibodies and detected with ECL as described above. Primary antibodies dilutions for dot blotting are as follows: anti-Aβ W0-2 (1:1.500), anti-Aβ40 (1:1.000), anti-Aβ42 (1:1.000). Secondary antibodies dilutions are as follows: anti-mouse (1:10.000) or anti-rabbit (1:10.000). Both primary and secondary antibodies were diluted in 0.1% PBS-Tween.

For native gels, the samples were harvested and prepared in native sample buffer and run on Novex Tris–Glycine gels (ThermoFisher) in native running buffer as per the manufacturer's instructions (https://www.thermofisher.com/uk/en/home/life-science/protein-biology/protein-gel-electrophoresis/protein-gels/novex-tris-glycine-gels.html). From here, the transfer and detection of the membrane were as described above. Membranes were detected with the W0-2 and anti-Cter antibodies at the same dilutions stated above.

Full-length images of cropped gels presented in the main figures are provided in the Supplemental Data file. We have highlighted instances in which the membrane was cut prior to antibody binding and detection, particularly in the case of Actin detections. Regardless, we still provide the full-length original images of the samples presented in the main figures.

Isolation of Aβ assemblies: gel eluted liquid fraction entrapment electrophoresis (GELFrEE). 6.6×10^6 CHO cells were seeded in T175 flasks 24 h before transfection. Cells were transfected with 45 µg of DNA using Lipofectamine 2000 and a 0% FBS medium change was carried out 24 h after transfection. The media were harvested and lyophilised 48 h after initial transfection and resuspended in 1 ml milli-Q water. Aβ was immunoprecipitated using Sepharose A beads (Invitrogen) coated with the anti-Aβ W0-2 antibody. For immunoprecipitation, 100 µl recombinant Sepharose A beads (50 mg/ml) were incubated with the medium for 3 h as a pre-clearing step. This was then centrifuged at > 15.000 g for 5 min and the beads were discarded. The supernatant was next incubated with 5 µl W0-2 antibody for 1 h at 4 °C, after which 100 µl fresh Sepharose beads were added and incubated at 4 °C overnight. The beads were then washed 3 times with mQ water and resuspended in 104 µl mQ water, 16 µl of DTT 0.5 M and 30 µl Tris–Acetate loading buffer. The mixture was boiled at 95 °C for 10 min and centrifuged at > 15.000 g for 5 min. The supernatant was loaded into the GELFrEE 8100 system and run using the following method; Step 1- 16 min at 50 V, Step 2- 40 min at 50 V (Monomer fraction), Step 3- 4 min at 50 V, Step 4- 6 min at 70 V, Step 4- 13 min at 85 V and Step 6- 38 min at 85 V (Hexamer Fraction).

Samples were collected in the system running buffer (1X buffer; 1% HEPES, 0.01% EDTA, 0.1% SDS and 0.1% Tris) and kept on ice. The monomeric fraction was then put through a buffer equilibrated 7 K MWCO Zeba buffer-exchange column (Thermo Scientific) to remove the Tris–Acetate blue sample buffer. The absorbance at 280 nm was read using a BioPhotometer D30 (Eppendorf) and the concentration of the collected Aβ assemblies were calculated using the molecular coefficient of 1490 M-1 cm-1; $(A280/1490) \times 1000 \times 1000$.

For assembly over time experiments, monomeric and hexameric samples were incubated at room temperature and 20 µl aliquots were taken for western blotting at each time point.

ECLIA. Quantification of $A\beta_{38}$, $A\beta_{40}$, and $A\beta_{42}$ monomeric peptides in the serum free media of C99 transfected CHO cells was achieved using the Aβ multiplex electro-chemiluminescence immunoassay (ECLIA; Meso Scale Discovery, Gaithersburg, MD, USA) as previously described[64]. Aβ were quantified with the human Aβ specific 6E10 multiplex assay according to the manufacturer's instructions.

Synthetic monomeric Aβ preparation and seeding. Monomeric solutions of Aβ were prepared as previously described[45,47]. Briefly, recombinant Aβ40 and Aβ42 were purchased from rPeptide as 1,1,1,3,3,3-Hexafluoro-2-propanol (HFIP) films. 0.2 mg aliquots of peptide were solubilised in 200 µl HFIP (Sigma-Aldrich) to disaggregate any preformed aggregates. The solution was then vortexed for 1 min and sonicated in a water bath for 5 min. The HFIP was then dried off using a steady flow of nitrogen gas. 200 µl of anhydrous dimethyl sulfoxide (DMSO) (Sigma-Aldrich) was then added and the solution was vortexed for 1 min. The solution was then put through a buffer equilibrated 7 K MWCO Zeba buffer-exchange column (Thermo Scientific) at 4 °C. The protein solution was then kept on ice whilst the absorbance at 280 nm was measured using a BioPhotometer D30 (Eppendorf) spectrophotometer. The concentration was calculated using the molecular coefficient of 1490 M-1 cm-1; $(A280/1490) \times 1000 \times 1000$. Solutions were immediately diluted to 50 µM in buffer and this was taken to be the new working stock.

ThT assay. To assess the self-assembly of the isolated hexameric Aβ, the fluorescence of 20 µM ThT (Sigma-Aldrich) in 150 µM isolated hexamer was measured over 48 h in 96 well plates using the VICTOR Multilabel Plate Reader (PerkinElmer, Waltham, MA, USA). For seeding experiments, fluorescence of 20 µM ThT in 50 µM monomeric Aβ40 or Aβ42 was monitored over 24 h. Fluorescence readings were obtained at room temperature with excitation and emission wavelengths set at 460 nm and 483 nm respectively.

Mass spectrometry. The fractions of the cellular samples from the GELFrEE system were passed through HiPPR Detergent Removal 0.1 ml columns (ThermoFisher Scientific), previously equilibrated with a 25 mM ammonium bicarbonate (NH_4HCO_3) solution, to remove the detergent from the solution. The samples were centrifuged for 2 min at 1500 g, then lyophilised.

Samples were then resuspended in 50 mM ammonium bicarbonate before being first reduced (10 mM dithiothreitol) for 40 min at 56 °C, alkylated (20 mM iodoacetamide) for 30 min at room temperature, and finally digested with trypsin for 16 h at 37 °C (1/50 w/w enzyme/proteins ratio). Reactions were stopped by acidifying the solution using 10% TFA. Generated peptides were then analyzed by LC–MS/MS.

Peptides were separated by reversed-phase chromatography using Ultra Performance Liquid Chromatography (UPLC-MClass, HSS T3 column, Waters, Milford, MA, USA) in one dimension with a linear gradient of acetonitrile (5 to 40% in 70 min, solvent A was water 0.1% formic acid, solvent B was acetonitrile 0.1% formic acid) at a 600 nl/min flow rate. The chromatography system was coupled with a Thermo Scientific Q Exactive Plus hybrid quadrupole-Orbitrap mass spectrometer (ThermoFisher Scientific, Waltham, MA, USA), with a targeted method. The targeted masses are the m/z of the three following doubly charged peptides, that result from the trypsin digestion: LVFFAEDVGSNK m/z 663.3404, GAIIGLMVGGVV m/z 543.3230 and GAIIGLMVGGVVIA m/z 635.3836.

Full-MS scans were acquired at 70.000 mass resolving power (full width at half maximum). A mass range from 400 to 1750 m/z was acquired in MS mode, and 3×10^6 ions were accumulated. Ion trap Higher energy Collision Dissociation fragmentations at NCE (Normalized Collision Energy) 25 were performed within 2amu isolation windows.

Raw MS files were analyzed by Proteome Discoverer 2.1.1.21 software (Thermo Scientific). MS/MS spectra were compared to the Uniprot *Cricetulus griseus* protein database, in which had been added the sequence of two main human amyloid peptides Aβ40 and Aβ42. Due to this restricted length in amino acids, the criteria for identification of each protein has been set up to one unique peptide per protein. The false discovery rate (FDR)

was set to 0.01 on both protein and peptide levels. The tolerance on mass accuracy was set at 5 ppm (10 ppm for MS/MS).

qPCR. RNAs were extracted from cells in TRIPure reagent and reverse-transcribed using an iScript cDNA synthesis kit. qPCR conditions were 95 °C for 30secs, followed by 40 cycles of 30secs at 95 °C, 45secs at 60 °C and 15secs at 79 °C and ended by 1 cycle of 15secs at 79 °C and 30secs at 60 °C. The relative changes in the target gene-to-GAPDH mRNA ratio were determined by the $2^{(-\Delta\Delta Ct)}$ calculation. The sequences for qPCR primers are provided in Supplemental Table S3.

Data availability

The datasets generated during and/or analysed during the current study are available from the corresponding author on reasonable request.

Received: 15 December 2020; Accepted: 4 May 2021
Published online: 02 June 2021

References

1. Selkoe, D. J. & Hardy, J. The amyloid hypothesis of Alzheimer's disease at 25 years. *EMBO Mol. Med.* **8**, 595–608. https://doi.org/10.15252/emmm.201606210 (2016).
2. Takami, M. *et al.* gamma-Secretase: successive tripeptide and tetrapeptide release from the transmembrane domain of beta-carboxyl terminal fragment. *J. Neurosci.* **29**, 13042–13052. https://doi.org/10.1523/JNEUROSCI.2362-09.2009 (2009).
3. Qi-Takahara, Y. *et al.* Longer forms of amyloid beta protein: implications for the mechanism of intramembrane cleavage by gamma-secretase. *J. Neurosci.* **25**, 436–445. https://doi.org/10.1523/JNEUROSCI.1575-04.2005 (2005).
4. Bolduc, D. M., Montagna, D. R., Seghers, M. C., Wolfe, M. S. & Selkoe, D. J. The amyloid-beta forming tripeptide cleavage mechanism of gamma-secretase. *Elife* https://doi.org/10.7554/eLife.17578 (2016).
5. Serpell, L. C. Alzheimer's amyloid fibrils: structure and assembly. *Biochim. Biophys. Acta* **1502**, 16–30. https://doi.org/10.1016/s0925-4439(00)00029-6 (2000).
6. Selkoe, D. J. Alzheimer's disease: a central role for amyloid. *J. Neuropathol. Exp. Neurol.* **53**, 438–447. https://doi.org/10.1097/00005072-199409000-00003 (1994).
7. Benilova, I., Karran, E. & De Strooper, B. The toxic Abeta oligomer and Alzheimer's disease: an emperor in need of clothes. *Nat. Neurosci.* **15**, 349–357. https://doi.org/10.1038/nn.3028 (2012).
8. McLean, C. A. *et al.* Soluble pool of Abeta amyloid as a determinant of severity of neurodegeneration in Alzheimer's disease. *Ann. Neurol.* **46**, 860–866. https://doi.org/10.1002/1531-8249(199912)46:6%3c860::aid-ana8%3e3.0.co;2-m (1999).
9. Jongbloed, W. *et al.* Amyloid-beta oligomers relate to cognitive decline in Alzheimer's disease. *J. Alzheimers Dis.* **45**, 35–43. https://doi.org/10.3233/JAD-142136 (2015).
10. Amar, F. *et al.* The amyloid-beta oligomer Abeta*56 induces specific alterations in neuronal signaling that lead to tau phosphorylation and aggregation. *Sci. Signal* https://doi.org/10.1126/scisignal.aal2021 (2017).
11. Lesne, S. E. *et al.* Brain amyloid-beta oligomers in ageing and Alzheimer's disease. *Brain* **136**, 1383–1398. https://doi.org/10.1093/brain/awt062 (2013).
12. Ladiwala, A. R. *et al.* Conformational differences between two amyloid beta oligomers of similar size and dissimilar toxicity. *J. Biol. Chem.* **287**, 24765–24773. https://doi.org/10.1074/jbc.M111.329763 (2012).
13. Broersen, K., Rousseau, F. & Schymkowitz, J. The culprit behind amyloid beta peptide related neurotoxicity in Alzheimer's disease: oligomer size or conformation?. *Alzheimers Res. Ther.* **2**, 12. https://doi.org/10.1186/alzrt36 (2010).
14. Deshpande, A., Mina, E., Glabe, C. & Busciglio, J. Different conformations of amyloid beta induce neurotoxicity by distinct mechanisms in human cortical neurons. *J. Neurosci.* **26**, 6011–6018. https://doi.org/10.1523/JNEUROSCI.1189-06.2006 (2006).
15. Lambert, M. P. *et al.* Diffusible, nonfibrillar ligands derived from Abeta1-42 are potent central nervous system neurotoxins. *Proc. Natl. Acad. Sci. USA.* **95**, 6448–6453. https://doi.org/10.1073/pnas.95.11.6448 (1998).
16. Townsend, M., Shankar, G. M., Mehta, T., Walsh, D. M. & Selkoe, D. J. Effects of secreted oligomers of amyloid beta-protein on hippocampal synaptic plasticity: a potent role for trimers. *J. Physiol.* **572**, 477–492. https://doi.org/10.1113/jphysiol.2005.103754 (2006).
17. Shankar, G. M. *et al.* Natural oligomers of the Alzheimer amyloid-beta protein induce reversible synapse loss by modulating an NMDA-type glutamate receptor-dependent signaling pathway. *J. Neurosci.* **27**, 2866–2875. https://doi.org/10.1523/JNEUROSCI.4970-06.2007 (2007).
18. Shankar, G. M. *et al.* Amyloid-beta protein dimers isolated directly from Alzheimer's brains impair synaptic plasticity and memory. *Nat. Med.* **14**, 837–842. https://doi.org/10.1038/nm1782 (2008).
19. Ferrone, F. Analysis of protein aggregation kinetics. *Methods Enzymol.* **309**, 256–274. https://doi.org/10.1016/s0076-6879(99)09019-9 (1999).
20. Roychaudhuri, R., Yang, M., Hoshi, M. M. & Teplow, D. B. Amyloid beta-protein assembly and Alzheimer disease. *J. Biol. Chem.* **284**, 4749–4753. https://doi.org/10.1074/jbc.R800036200 (2009).
21. Scheidt, T. *et al.* Secondary nucleation and elongation occur at different sites on Alzheimer's amyloid-beta aggregates. *Sci. Adv.* **5**, eaau3112. https://doi.org/10.1126/sciadv.aau3112 (2019).
22. Bernstein, S. L. *et al.* Amyloid-beta protein oligomerization and the importance of tetramers and dodecamers in the aetiology of Alzheimer's disease. *Nat. Chem.* **1**, 326–331. https://doi.org/10.1038/nchem.247 (2009).
23. Bitan, G. *et al.* Amyloid beta -protein (Abeta) assembly: Abeta 40 and Abeta 42 oligomerize through distinct pathways. *Proc. Natl. Acad. Sci. USA.* **100**, 330–335. https://doi.org/10.1073/pnas.222681699 (2003).
24. Cernescu, M. *et al.* Laser-induced liquid bead ion desorption mass spectrometry: an approach to precisely monitor the oligomerization of the beta-amyloid peptide. *Anal. Chem.* **84**, 5276–5284. https://doi.org/10.1021/ac300258m (2012).
25. Ono, K., Condron, M. M. & Teplow, D. B. Structure-neurotoxicity relationships of amyloid beta-protein oligomers. *Proc. Natl. Acad. Sci. USA.* **106**, 14745–14750. https://doi.org/10.1073/pnas.0905127106 (2009).
26. Bitan, G., Lomakin, A. & Teplow, D. B. Amyloid beta-protein oligomerization: prenucleation interactions revealed by photo-induced cross-linking of unmodified proteins. *J. Biol. Chem.* **276**, 35176–35184. https://doi.org/10.1074/jbc.M102223200 (2001).
27. Bitan, G. & Teplow, D. B. Rapid photochemical cross-linking–a new tool for studies of metastable, amyloidogenic protein assemblies. *Acc. Chem. Res.* **37**, 357–364. https://doi.org/10.1021/ar000214l (2004).
28. Wolff, M. *et al.* Abeta42 pentamers/hexamers are the smallest detectable oligomers in solution. *Sci. Rep.* **7**, 2493. https://doi.org/10.1038/s41598-017-02370-3 (2017).
29. Lesne, S. *et al.* A specific amyloid-beta protein assembly in the brain impairs memory. *Nature* **440**, 352–357. https://doi.org/10.1038/nature04533 (2006).

30. Bolognesi, B. *et al.* Single point mutations induce a switch in the molecular mechanism of the aggregation of the Alzheimer's disease associated Abeta42 peptide. *ACS Chem. Biol.* **9**, 378–382. https://doi.org/10.1021/cb400616y (2014).
31. Luheshi, L. M. *et al.* Systematic in vivo analysis of the intrinsic determinants of amyloid Beta pathogenicity. *PLoS Biol.* **5**, e290. https://doi.org/10.1371/journal.pbio.0050290 (2007).
32. Peralvarez-Marin, A. *et al.* Influence of residue 22 on the folding, aggregation profile, and toxicity of the Alzheimer's amyloid beta peptide. *Biophys. J.* **97**, 277–285. https://doi.org/10.1016/j.bpj.2009.04.017 (2009).
33. Johansson, A. S. *et al.* Physiochemical characterization of the Alzheimer's disease-related peptides A beta 1–42Arctic and A beta 1–42wt. *FEBS J.* **273**, 2618–2630. https://doi.org/10.1111/j.1742-4658.2006.05263.x (2006).
34. Yang, X. *et al.* On the role of sidechain size and charge in the aggregation of Abeta42 with familial mutations. *Proc. Natl. Acad. Sci. USA.* **115**, E5849–E5858. https://doi.org/10.1073/pnas.1803539115 (2018).
35. Ahmed, M. *et al.* Structural conversion of neurotoxic amyloid-beta(1–42) oligomers to fibrils. *Nat. Struct. Mol. Biol.* **17**, 561–567. https://doi.org/10.1038/nsmb.1799 (2010).
36. Melchor, J. P., McVoy, L. & Van Nostrand, W. E. Charge alterations of E22 enhance the pathogenic properties of the amyloid beta-protein. *J. Neurochem.* **74**, 2209–2212. https://doi.org/10.1046/j.1471-4159.2000.0742209.x (2000).
37. Murakami, K. *et al.* Synthesis, aggregation, neurotoxicity, and secondary structure of various A beta 1–42 mutants of familial Alzheimer's disease at positions 21–23. *Biochem. Biophys. Res. Commun.* **294**, 5–10. https://doi.org/10.1016/S0006-291X(02)00430-8 (2002).
38. Murakami, K. *et al.* Neurotoxicity and physicochemical properties of Abeta mutant peptides from cerebral amyloid angiopathy: implication for the pathogenesis of cerebral amyloid angiopathy and Alzheimer's disease. *J. Biol. Chem.* **278**, 46179–46187. https://doi.org/10.1074/jbc.M301874200 (2003).
39. Grabowski, T. J., Cho, H. S., Vonsattel, J. P., Rebeck, G. W. & Greenberg, S. M. Novel amyloid precursor protein mutation in an Iowa family with dementia and severe cerebral amyloid angiopathy. *Ann. Neurol.* **49**, 697–705. https://doi.org/10.1002/ana.1009 (2001).
40. Hendriks, L. *et al.* Presenile dementia and cerebral haemorrhage linked to a mutation at codon 692 of the beta-amyloid precursor protein gene. *Nat. Genet.* **1**, 218–221. https://doi.org/10.1038/ng0692-218 (1992).
41. Miravalle, L. *et al.* Substitutions at codon 22 of Alzheimer's abeta peptide induce diverse conformational changes and apoptotic effects in human cerebral endothelial cells. *J. Biol. Chem.* **275**, 27110–27116. https://doi.org/10.1074/jbc.M003154200 (2000).
42. Nilsberth, C. *et al.* The "Arctic" APP mutation (E693G) causes Alzheimer's disease by enhanced Abeta protofibril formation. *Nat. Neurosci.* **4**, 887–893. https://doi.org/10.1038/nn0901-887 (2001).
43. Decock, M. *et al.* Glycines from the APP GXXXG/GXXXA transmembrane motifs promote formation of pathogenic abeta oligomers in cells. *Front. Aging Neurosci.* **8**, 107. https://doi.org/10.3389/fnagi.2016.00107 (2016).
44. Pujol-Pina, R. *et al.* SDS-PAGE analysis of Abeta oligomers is disserving research into Alzheimer s disease: appealing for ESI-IM-MS. *Sci. Rep.* **5**, 14809. https://doi.org/10.1038/srep14809 (2015).
45. Marshall, K. E. *et al.* A critical role for the self-assembly of Amyloid-beta1-42 in neurodegeneration. *Sci. Rep.* **6**, 30182. https://doi.org/10.1038/srep30182 (2016).
46. Jarrett, J. T., Berger, E. P. & Lansbury, P. T. Jr. The carboxy terminus of the beta amyloid protein is critical for the seeding of amyloid formation: implications for the pathogenesis of Alzheimer's disease. *Biochemistry* **32**, 4693–4697. https://doi.org/10.1021/bi00069a001 (1993).
47. Broersen, K. *et al.* A standardized and biocompatible preparation of aggregate-free amyloid beta peptide for biophysical and biological studies of Alzheimer's disease. *Protein Eng. Des. Sel.* **24**, 743–750. https://doi.org/10.1093/protein/gzr020 (2011).
48. Vadukul, D. M., Gbajumo, O., Marshall, K. E. & Serpell, L. C. Amyloidogenicity and toxicity of the reverse and scrambled variants of amyloid-beta 1–42. *FEBS Lett.* **591**, 822–830. https://doi.org/10.1002/1873-3468.12590 (2017).
49. Osterlund, N., Moons, R., Ilag, L. L., Sobott, F. & Graslund, A. Native ion mobility-mass spectrometry reveals the formation of beta-barrel shaped amyloid-beta Hexamers in a membrane-mimicking environment. *J. Am. Chem. Soc.* **141**, 10440–10450. https://doi.org/10.1021/jacs.9b04596 (2019).
50. Cukalevski, R. *et al.* Role of aromatic side chains in amyloid beta-protein aggregation. *ACS Chem. Neurosci.* **3**, 1008–1016. https://doi.org/10.1021/cn300073s (2012).
51. Esler, W. P. *et al.* Point substitution in the central hydrophobic cluster of a human beta-amyloid congener disrupts peptide folding and abolishes plaque competence. *Biochemistry* **35**, 13914–13921. https://doi.org/10.1021/bi961302+ (1996).
52. Hilbich, C., Kisters-Woike, B., Reed, J., Masters, C. L. & Beyreuther, K. Substitutions of hydrophobic amino acids reduce the amyloidogenicity of Alzheimer's disease beta A4 peptides. *J. Mol. Biol.* **228**, 460–473. https://doi.org/10.1016/0022-2836(92)90835-8 (1992).
53. Wurth, C., Guimard, N. K. & Hecht, M. H. Mutations that reduce aggregation of the Alzheimer's Abeta42 peptide: an unbiased search for the sequence determinants of Abeta amyloidogenesis. *J. Mol. Biol.* **319**, 1279–1290. https://doi.org/10.1016/S0022-2836(02)00399-6 (2002).
54. Gazit, E. A possible role for pi-stacking in the self-assembly of amyloid fibrils. *FASEB J.* **16**, 77–83. https://doi.org/10.1096/fj.01-0442hyp (2002).
55. Masuda, Y. *et al.* Verification of the turn at positions 22 and 23 of the beta-amyloid fibrils with Italian mutation using solid-state NMR. *Bioorg. Med. Chem.* **13**, 6803–6809. https://doi.org/10.1016/j.bmc.2005.07.071 (2005).
56. Murakami, K. *et al.* Formation and stabilization model of the 42-mer Abeta radical: implications for the long-lasting oxidative stress in Alzheimer's disease. *J. Am. Chem. Soc.* **127**, 15168–15174. https://doi.org/10.1021/ja054041c (2005).
57. Roychaudhuri, R., Yang, M., Condron, M. M. & Teplow, D. B. Structural dynamics of the amyloid beta-protein monomer folding nucleus. *Biochemistry* **51**, 3957–3959. https://doi.org/10.1021/bi300350p (2012).
58. Grant, M. A. *et al.* Familial Alzheimer's disease mutations alter the stability of the amyloid beta-protein monomer folding nucleus. *Proc. Natl. Acad. Sci. USA.* **104**, 16522–16527. https://doi.org/10.1073/pnas.0705197104 (2007).
59. Lazo, N. D., Grant, M. A., Condron, M. C., Rigby, A. C. & Teplow, D. B. On the nucleation of amyloid beta-protein monomer folding. *Protein Sci.* **14**, 1581–1596. https://doi.org/10.1110/ps.041292205 (2005).
60. Krone, M. G. *et al.* Effects of familial Alzheimer's disease mutations on the folding nucleation of the amyloid beta-protein. *J. Mol. Biol.* **381**, 221–228. https://doi.org/10.1016/j.jmb.2008.05.069 (2008).
61. Karamanos, T. K. *et al.* Structural mapping of oligomeric intermediates in an amyloid assembly pathway. *Elife* https://doi.org/10.7554/eLife.46574 (2019).
62. Kienlen-Campard, P. *et al.* Amyloidogenic processing but not amyloid precursor protein (APP) intracellular Cterminal domain production requires a precisely oriented APP dimer assembled by transmembrane GXXXG motifs. *J. Biol. Chem.* **283**, 7733–7744. https://doi.org/10.1074/jbc.M707142200 (2008).
63. Ben Khalifa, N. *et al.* Structural features of the KPI domain control APP dimerization, trafficking, and processing. *FASEB J.* **26**, 855–867. https://doi.org/10.1096/fj.11-190207 (2012).
64. Hage, S. *et al.* Characterization of Pterocarpus erinaceus kino extract and its gamma-secretase inhibitory properties. *J. Ethnopharmacol.* **163**, 192–202. https://doi.org/10.1016/j.jep.2015.01.028 (2015).

Acknowledgements
The authors thank Esther Paître and Pierre Burguet for their technical support. We also thank Loic Quinton for kindly providing us with the Gel Eluted Liquid Fraction Entrapment Electrophoresis (GELFrEE) 8100 system. Funding to P.K.C is acknowledged from SAO-FRA Alzheimer Research Foundation, Fondation Louvain and Queen Elisabeth Medical Research Foundation (FMRE to P.K.C and LQ). The work was supported by funds from FNRS grant PDRT.0177.18 to P.K.C and LQ.

Author contributions
D.M.V. designed and performed research, analysed data and wrote the manuscript. C.V. performed research and analysed data. P.B. performed mass spectrometry experiments under the supervision of L.Q. N.S. and S.C. analysed and interpreted data. L.C.S. kindly provided us with the vAβ sequence and provided guidance with interpretation of data. P.K.C. supervised, designed research project and interpretations. All authors reviewed the manuscript.

Competing interests
The authors declare no competing interests.

Additional information
Supplementary Information The online version contains supplementary material available at https://doi.org/10.1038/s41598-021-90680-y.

Correspondence and requests for materials should be addressed to P.K.-C.

Reprints and permissions information is available at www.nature.com/reprints.

Publisher's note Springer Nature remains neutral with regard to jurisdictional claims in published maps and institutional affiliations.